University of Reading

Deciphering human influence on annual maximum flood extent at the global level

Article

Published Version

Creative Commons: Attribution 4.0 (CC-BY)

Open Access

Mazzoleni, M., Dottori, F., Cloke, H. L. ORCID: https://orcid.org/0000-0002-1472-868X and Di Baldassarre, G. (2022) Deciphering human influence on annual maximum flood extent at the global level. Communications Earth & Environment, 3 (1). 262. ISSN 2662-4435 doi: 10.1038/s43247-022-00598-0 Available at https://centaur.reading.ac.uk/108457/

It is advisable to refer to the publisher's version if you intend to cite from the work. See Guidance on citing.

To link to this article DOI: http://dx.doi.org/10.1038/s43247-022-00598-0

Publisher: Springer Nature

All outputs in CentAUR are protected by Intellectual Property Rights law, including copyright law. Copyright and IPR is retained by the creators or other copyright holders. Terms and conditions for use of this material are defined in the End User Agreement.

www.reading.ac.uk/centaur

University of Reading

CentAUR

Central Archive at the University of Reading

Reading's research outputs online

communications earth & environment

ARTICLE

https://doi.org/10.1038/s43247-022-00598-0 OPEN

Deciphering human influence on annual maximum flood extent at the global level

Maurizio Mazzoleni [1,2]✉, Francesco Dottori [3], Hannah L. Cloke[2,4,5,6] & Giuliano Di Baldassarre[2,4]

Human actions are increasingly altering most river basins worldwide, resulting in changes in hydrological processes and extreme events. Yet, global patterns of changes between seasonal surface water and urbanization remain largely unknown. Here we perform a worldwide analysis of 106 large river basins and uncover global trends of annual maximum flood extent and artificial impervious area, as proxy of urbanization, over the past three decades. We explore their relationships with hydroclimatic variability, expressed as rainfall and snowmelt, and find that hydroclimatic variability alone cannot explain changes in annual maximum flood extent in 75% of the analyzed major river basins worldwide. Considering rainfall and urban area together can explain changes in the annual maximum flood extent in 57% of the basins. Our study emphasizes the importance of understanding the global impacts of human presence on changes in seasonal water dynamics.

[1] Institute for Environmental Studies, Vrije Universiteit Amsterdam, Amsterdam, the Netherlands. [2] Centre of Natural Hazards and Disaster Science (CNDS), Uppsala, Sweden. [3] European Commission, Joint Research Centre, Ispra, Italy. [4] Department of Earth Sciences, Uppsala University, Uppsala, Sweden. [5] Department of Geography and Environmental Science, University of Reading, Reading, UK. [6] Department of Meteorology, University of Reading, Reading, UK. ✉email: m.mazzoleni@vu.nl

Anthropogenic climate change is drastically changing the spatio-temporal climatic patterns[1], leading to changes in the timing and duration of hydrological extremes at the global scale[2,3]. Intensification of extreme precipitation and flood events have been observed worldwide[4]. As a result, ordinary high-water conditions and thus annual seasonal surface water extent (annual maximum flood extent, AMFE, hereafter) have increased more than permanent surface water area over the past three decades[5,6].

Together with climatic variability, human presence has altered the hydrological response of river basins over the last decades, through land cover changes[7], agricultural irrigation[8], and dam construction[9,10]. Lower infiltration due to land-use changes increases surface runoff, and together with changes in flow conveyance characteristics leads to higher flood peaks and larger flooding extents[11–13]. Similarly, agricultural practice, drainage, terracing, and forest change cause soil compaction and decrease soil infiltration. While dams have enabled societies to reduce flooding risk and exposure[14], they are strongly influencing the variability of global seasonal surface water, greenhouse emissions[15], and degraded water quality and ecosystems[10].

Unprecedented rates of global urbanization[16,17] have significantly shaped the hydrological response and water availability in most river basins around the world[18–20]. Land-use changes and urbanization driven by socio-economic factors have deeply contributed to increasing flood risk and exacerbating economic losses and human exposure[21–23]. Urbanization patterns have been shown to affect the severity of flood extent worldwide, e.g., in several African cities, Brazil, Canada, China, Indonesia, Italy, Peru, United Kingdom, and United States[19,24–29].

Changes in AMFE are important indicators for both ordinary high-water conditions and water availability. Understanding the influence of increasing global urbanization trends on AMFE is of pivotal importance for preserving inland water ecosystems[30] and guaranteeing freshwater sources for agriculture, water supply[31], and electricity production[32]. Changes in the availability of seasonal surface water can also lead to different impacts on society and ecosystems at different scales[6]. For these reasons, understanding changes in AMFE will enable the support of better-informed decision-making and disaster risk reduction policies for strengthening resilience and adaptive capacity[33].

A number of studies have investigated the influence of changes in the urbanized area on particular extreme flooding events using statistical and modeling frameworks. These studies found increasing flood extent and consequent impacts due to urbanization. Studies using statistical flood-frequency analyses have investigated the relationship between changes in impervious surfaces with changing flood magnitude and timing, both for single river basins or paired basins with different urban growths[28,34,35]. Models have been used to estimate the impact of land-use change and type of impervious area on flood frequency and magnitude by carefully setting the model parameter values[36,37]. The use of modeling tools enabled a more accurate spatio-temporal representation of flood processes, showing that increasing impervious area could also affect rural and peri-urban areas and not only, as expected, urban areas[38].

Despite these previous efforts aimed at quantifying the relation between urbanization and extreme flooding events at local to regional scales, it is still unclear how human presence has influenced the occurrence of seasonal surface water, i.e., AMFE (the focus of this study), over the last decades at the global scale. In this study we explore the long spatio-temporal evolution of global AMFE and impervious area, as proxy of urbanization, using high-resolution observational global data over the last 30 years. In particular, we investigate the relation between changes in the AMFE and changes in the hydroclimatic variables and urban area. To address these objectives, we first investigate the concurrent trends of AMFE and artificial urban area as proxy of human activities. Then, multiple regression models are implemented to assess the influence of urban area and hydroclimatic variables such as rainfall and snowmelt on the variability of AMFE. We exploit multiple high-resolution global datasets to represent AMFE, urban area, rainfall and snowmelt, floodplain delineation, and reservoir maximum storage capacity in the period 1985–2018.

Results

Global trends of annual maximum flood extent. AMFE—the maximum extent of water overflowing onto areas that are usually dry—was estimated as seasonal maximum surface water, i.e., present for only part of the year, from the Global Surface Water dataset[5] (see "Methods"). A total of 106 river basins were selected based on floodplain location and drainage area size. The trend analysis reveals a general increase in the AMFE within floodplains worldwide (Fig. 1a). Global trends range from a decrease of $-1.7\%\,yr^{-1}$ (Sao Francisco river basin, Brazil) to an increase of $8.1\%\,yr^{-1}$ (Rharsa river basin, Tunisia) per year. Significant trends at the 0.05-level are found for 77 out of 106 river basins, and visualized with a dot in Fig. 1a. The empirical distribution of the trend values (Fig. 1b) shows an average value of about 2.8.

The highest change rates are found in river basins located in Africa and Asia, with average continental values equal to 5.0 and 3.1, respectively. Conversely, North America, Central America, and the Caribbean area show the lowest average trend value equal to 1.1, followed by South America with an average value of 1.27. Similar high increases in surface water area in river basins in US and China were also recently observed in other studies[39,40]. Europe and South-West Pacific area have average trend values of 2.4 and 2.2, respectively.

Among the major world river basins with high significant AMFE trend, we can find the Chad ($6.6\%\,yr^{-1}$), the Zambezi ($5.9\%\,yr^{-1}$), the Niger ($5.4\%\,yr^{-1}$), the Yellow ($5.1\%\,yr^{-1}$), the Congo ($4.7\%\,yr^{-1}$), the Nile ($4.5\%\,yr^{-1}$), and the Yangtze ($3.7\%\,yr^{-1}$) river basins. The Mississippi ($1.2\%\,yr^{-1}$), the Amazon ($0.93\%\,yr^{-1}$), and the Amur ($0.1\%\,yr^{-1}$) river basins show negligible trends of AMFE. On the other hand, only eight basins show a decreasing trend in the flooded area, with the Parana and Murray rivers having trends $-1.2\%\,yr^{-1}$ and $-0.5\%\,yr^{-1}$, respectively.

When analyzing the changes of AMFEs by different global hydroclimatic regions, the highest change rate values are found in equatorial basins, which could be linked to the high values of average rainfall (Supplementary Fig. 7) and runoff[41] in those basins. River basins located in the northern dry area show the highest spread in AMFE trends (Fig. 1c) mainly due to the contrasting values observed in the Rharsa ($8.1\%\,yr^{-1}$), Sarysu ($7.3\%\,yr^{-1}$), Ural ($-1.6\%\,yr^{-1}$), and the Great Salt Lake ($-0.9\%\,yr^{-1}$) river basins caused by the diverse latitude of these basins. The lowest values are found in southern mid-latitude and boreal basins.

Global trends of the annual urban area. Artificial impervious area is a critical indicator of impervious surfaces associated with urbanization and human settlements within river basins[42–44]. As such, in the following, we assume that artificial impervious area can be considered a proxy of the urban area. As was observed with the trends of AMFE, the extent of artificial impervious surface (urban area, hereafter) is also generally increasing worldwide (Fig. 2a). Our findings reveal a slightly lower average trend of urban area within the floodplains ($2.9\%\,yr^{-1}$) than

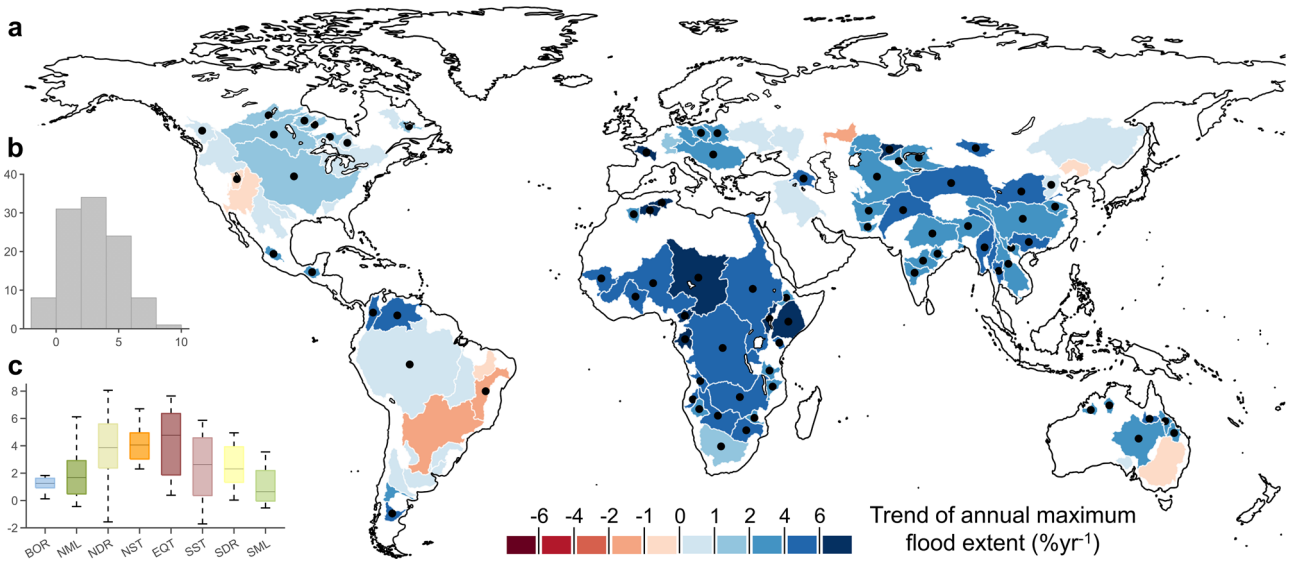

Fig. 1 Global trends of AMFE. a Theil–Sen slope trend of the AMFE normalized over the average value for the period 1985–2018. The black dots indicate a significant trend. **b** Distribution of the values of the trend of AMFE. **c** Boxplots of the trend of normalized AMFE for each hydroclimatic region, i.e., boreal (BOR), equatorial (EQT), northern mid-latitude (NML), southern mid-latitude (SML), northern dry (NDR), southern dry (SDR), northern sub-tropical (NST), southern sub-tropical (SST). Boxplot elements shown are the median (midline), the interquartile range of 25% and 75% percentile (box boundaries), and data points within the 1.5× quartile range (whiskers).

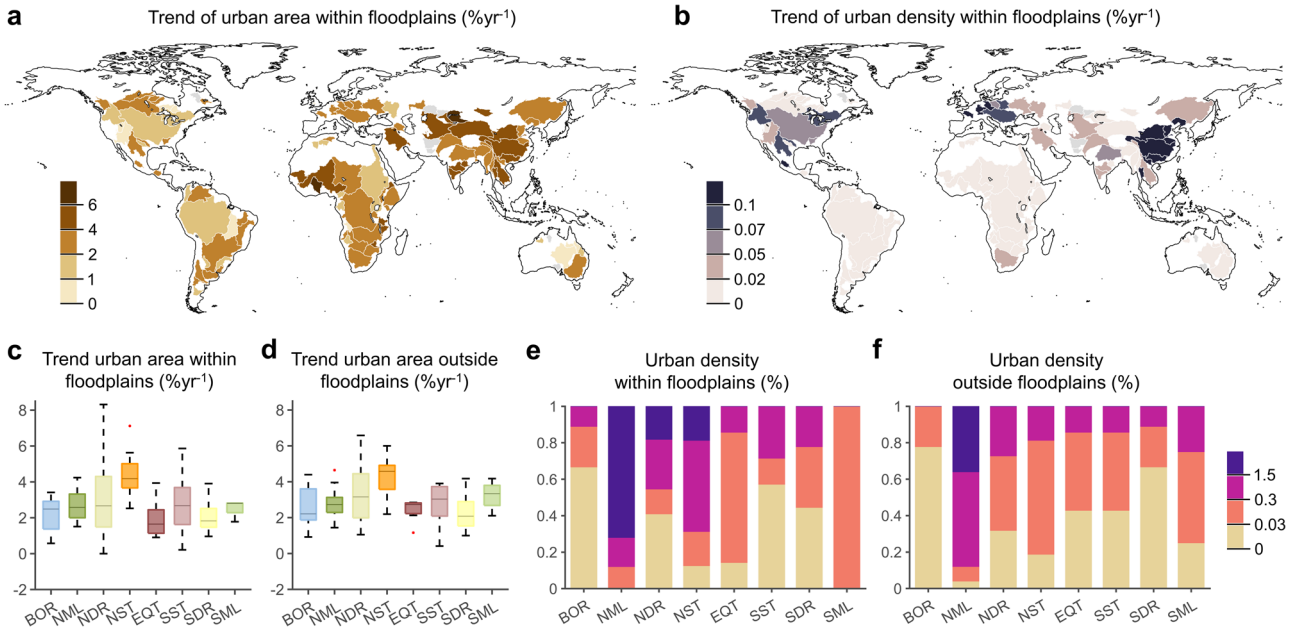

Fig. 2 Global trends of annual urban area and density of floodplain urbanization. Theil–Sen slope trends of the annual urban area normalized over the average value for the period 1985–2018 (**a**) and annual urban density (**b**) within the floodplains. Significant trends are found in all the river basins. **c**, **d** Boxplots of the trends of normalized annual urban area within and outside the floodplains for each hydroclimatic region, i.e., boreal (BOR), equatorial (EQT), northern mid-latitude (NML), southern mid-latitude (SML), northern dry (NDR), southern dry (SDR), northern sub-tropical (NST), southern sub-tropical (SST). Boxplot elements shown are the median (midline), the interquartile range of 25% and 75% percentile (box boundaries), data points within the 1.5× quartile range (whiskers), and outliers (red dots). **e**, **f** Fraction of basins belonging to different classes of urban density within and outside the floodplains for each hydroclimatic region.

outside (3.1% yr^{-1}). Maximum values of 8.3% yr^{-1} (Balkhash-Alakol Basin, Asia) within floodplains, and 8.7% yr^{-1} (Senegal river, Africa) outside the floodplains are observed. Similarly, the higher average urban area is found outside the floodplain than within (Supplementary Fig. 3a). In all the continents, the average value and annual trend of urban area is higher outside the river floodplains, with the exception of Asia that shows slightly higher values inside a few river floodplains.

Opposite results are found when analyzing the trends of urban density (Fig. 2b), calculated as the ratio between the annual urban area and floodplain area. Higher average trends of urban density are found within the floodplains (0.04% yr^{-1}) than outside (0.02% yr^{-1}), with maximum values of 0.5% yr^{-1} (Yongding basin, Asia) within floodplains, and 0.23% yr^{-1} (Huai He basin, Asia) outside. Higher average urban density values within floodplains than outside are found in all continents

(Supplementary Fig. 3b), with the exception of a few river basins such as the Parana, Rio de la Plata, Zambezi, Okavango, Limpopo, Orinoco, and Tarim He basins. This finding stresses once more the role of floodplains in promoting socio-economic growth and consequent urban expansion.

The highest increase of urban area within floodplains is found in Asian and African river basins (Fig. 2a), with an average country value of 4.0% yr^{-1} and 3.3% yr^{-1}, respectively. In those continents, the major river basins with high significant trends of urban area within floodplains are the Volta River (7.1% yr^{-1}), the Senegal river (4.9% yr^{-1}), the Niger River (4.3% yr^{-1}), the Mekong River (5.2% yr^{-1}), the Tarim river (5.9% yr^{-1}), and the Yangtze River (4.2% yr^{-1}). Europe shows an average trend value of urban area within the floodplains of 2.4% yr^{-1}, similar to the global average trend of AMFE.

River basins with high trends of urban density within the floodplains can be found in the United States, Europe, and East China. The lowest trends in urban density values are observed in South America, Australia, and Africa, which could be linked to the floodplain extent in relation to the total basin area (18.1%, 15.5%, and 15.8%, respectively) compared to Europe, North America, and Asia (14.8%, 11.7%, and 10.8%, respectively). These findings highlight the importance of considering the relative spatial extent of the artificial impervious surface when exploring urbanization effects. When focusing at basin scale, those that show higher positive values of trends in urban density within floodplains are the Rhine river (0.38% yr^{-1}), the Zhu river (0.33% yr^{-1}), the Yellow river (0.17% yr^{-1}), the Yangtze river (0.17% yr^{-1}), the Loire river (0.14% yr^{-1}), and the Rio Grande river (0.9% yr^{-1}).

Comparable changes in trends in an urban area within and outside the floodplains are obtained for global hydroclimatic regions (Fig. 2c, d). The highest average values are found in northern sub-tropical areas, while higher spread of trend values can be observed in a northern dry area. The lowest values are found in boreal and equatorial river basins. With respect to the average annual urban density (Fig. 2e, f), we observed that the majority of the basin with density higher than 1.5% belongs to the northern mid-latitude areas.

Concurrent trends analysis. Here, we compare the trends of AMFE with those of urban areas and density. These exploratory analyses provide further insights for the basins in which high increase of AMFE could be linked to growing floodplains urbanization.

A high increase in both trends of the urban area and AMFE (i.e., higher than the 75th percentile of the sample of the total trends of the urban area and AMFE, see Fig. 3) is observed in only nine river basins of the world, including the Volta, Senegal, Orinoco, Niger, Tarim, and Yellow River. On the other hand, high increase in both urban density and AMFE are found in three basins, i.e., in the Loire, Zhu, and Yellow River basins. Some general spatial patterns can be found at the global scale (Fig. 3a, b).

In Africa, AMFE tends to increase more than the urban area and density within floodplains. On the other hand, in Asia and South America, a lower and moderate increase in AMFE with a higher change in urban area and density can be observed. In Europe, both AMFE and urban area show moderate trends (middle class in Fig. 3a). Similar patterns can be found in the central and Eastern part of North America, while in the western basins AMFE seems to increase more slowly than in urban area. However, higher trends of urban density are experienced in European and North American basins. Major river basins such as the Amazon, the Okavango, and the Nile rivers show an increase in AMFE while a lower increase in urban area, while higher increase in urban density are experienced in the Mississippi river.

River basins that experienced both high changes in AMFE and urban area are mainly located in equatorial, northern dry and northern sub-tropical regions (Fig. 3c), while basins with high changes in AMFE and urban density are found in northern mid-latitude and areas (Fig. 3d). The majority of the river basins in the northern mid-latitude area shows a moderate increase in AMFE and urban area while a higher increase in urban density.

While urban surface and AMFE shows similar trends in many river basins worldwide, their occurrence at basin scale may be spatially uncorrelated. For this reason, we intersected the footprint of AMFE with the urban area to assess the annual flooded urban area within floodplains. We then calculated the annual trends of relative flooded urban area estimated as the ratio between annual flooded urban area and the annual urban area. Overall, the majority of the river basins experienced positive trends, showing that flooded urban area is increasing faster than urban area within floodplains (Fig. 3a, b). In particular, high trend values are found in river basins in Asia, and West and South Africa (e.g., on the Senegal, Mekong, Tarim, Yellow River, Niger, and Orinoco rivers). On the other hand, lower trends characterize basins in which either flooded urban area is increasing slower than urban area, as in some Europe basins with high urban density (e.g., in the Rhine basin), or in which both flooded urban area and urbanization are decreasing, as in some basins in North and South America (e.g., in the Columbia, and Amazon rivers, see Supplementary Fig. 5b). The trends of relative flooded urban area are then compared with that of AMFE. The pattern depicted in Fig. 3e shows a linear relation between trends in relative flooded urban area and AMFE. Higher values of trends in relative flooded urban area are also related to high trends of the urban area.

Hydroclimatic influence on annual maximum flood extent. Climate variability has significantly shaped changes in AMFE[45]. To explore the influence of hydroclimatic and anthropogenic factors, we assess the pair-wise correlation of AMFE with rainfall and snowmelt, at different temporal scales (i.e., annual maximum, monthly maximum, and total annual), and urban area. We did not consider river streamflow and soil moisture as dependent to changes in the urban area. Here we report the results considering monthly maximum rainfall and monthly maximum snowmelt (Fig. 4). Moreover, since the urban density is calculated as the urban area over the floodplain area, constant over time, identical correlation results were achieved. Thus, urban area is considered as explanatory variable in the following statistical analyses.

The findings highlight that the majority of the river basins shows a positive Spearman rank correlation of rainfall and snowmelt with AMFE (Fig. 4). In particular, 83 out of 106 basins have a positive correlation between rainfall and AMFE, with 74 basins reporting also a positive correlation between urban area and AMFE (Fig. 4a). A total of 23 river basins have a positive correlation with urban area and increasing trend of AMFE but a negative rainfall correlation (e.g., in the Red, Indus, Ogooue, Yangtze, Congo, and Nile rivers). These preliminary results suggest that, despite a negative correlation of precipitation (found mainly in equatorial, northern dry, and northern sub-tropical), an increasing AMFE could be due to a positive correlation with urban area.

Similar patterns are depicted between snowmelt and AMFE (Fig. 4b) with 60 basins showing a positive correlation. A total of 44 river basins shows a negative correlation between snowmelt and AMFE while a positive one with urban area. Among these basins, we can find the Sao Francisco, Orinoco, Yellow River,

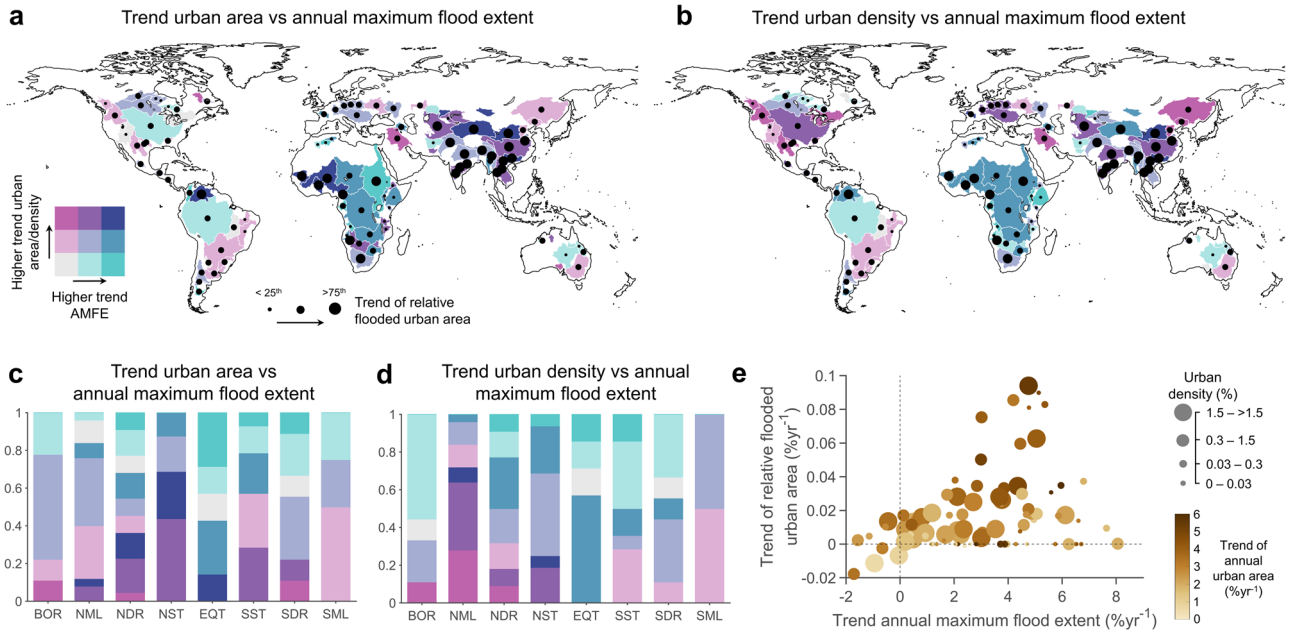

Fig. 3 Analysis of concurrent trends of AMFE, annual urban area, annual urban density, and annual flooded urban area. Bivariate maps between trend of normalized AMFE and trend of normalized annual urban area within the floodplains (**a**) and between trend of normalized AMFE and trend of annual urban density within the floodplains (**b**). The size of each black dot indicates whether the trend of a given basin falls below the 25th percentile, between the 25th and 75th percentiles, or above the 75th percentile of the sample of trends of normalized relative flooded urban area. **c**, **d** Fraction of basin belonging to different classes of the bivariate values for each hydroclimatic region in case urban area (**c**) or urban density (**d**) is considered. **e** Relation between the trend of normalized AMFE and trend of normalized relative flooded urban area. The colors of the scatter plots represent the trend of the normalized annual urban area, while the size of the scatter plot is the urban density within the floodplains.

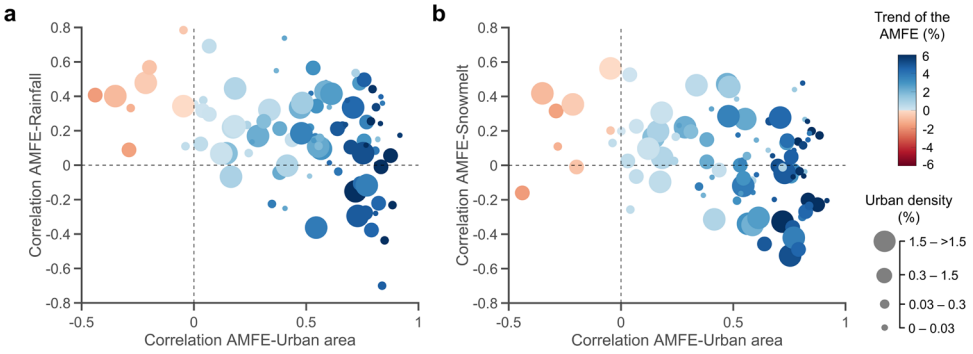

Fig. 4 Correlation analysis between AMFE, hydroclimatic variables, and urban area. Comparison of the Spearman rank correlation coefficients between AMFE and monthly maximum hydroclimatic variables (**a**, rainfall; **b**, snowmelt) and Spearman rank correlation coefficient between AMFE and the annual urban area within the river floodplains. The colors of the scatter plots represent the trend of then AMFE, while the size of the scatter plot is the urban density within the floodplains.

Ganges, Zambezi, Tarim, Yangtze, Chad, Congo, Nile, and Amazon rivers.

There is no apparent correlation pattern between rainfall, snowmelt, urban area, AMFE, and urban density within floodplains. Similar results are found when correlating annual maximum rainfall (and snowmelt) and total annual rainfall (and snowmelt) with AMFE (Supplementary Fig. 11). Despite the interesting outcomes of these analyses, the results cannot explain the compound influence of both hydroclimatic and anthropogenic factors on AMFE.

Influence of urban area, reservoirs, and hydroclimatic variables in explaining changes in annual maximum flood extent. River basins with large changes in maximum flood extent (Fig. 1a) do not necessarily show a similar increasing trend in rainfall and snowmelt (Fig. 4 and Supplementary Figs. 12 and 13). On the other hand, a significant increase of floodplain urban area is observed in those river basins (Fig. 2a). Two stepwise multiple linear regression analyses were performed to identify the response variables explaining the changes in the AMFE. First, only rainfall and snowmelt were considered as explanatory variables of the AMFE. Second, the floodplain urban area and reservoir maximum capacity were included to assess the human influence in shaping maximum flood extent.

The stepwise regression with only rainfall and snowmelt indicated a statistically significant correlation (0.05 level) with AMFE on 67 of the analyzed 106 river basins. When the contribution of urban area is neglected, AMFE is correlated with only rainfall drivers in 41 (62%) basins and with both rainfall and snowmelt in 25 (38%) basins (Figs. 5a and 6). Values of adjusted R^2 higher than 0.5 are found in on the Colorado, Murray, Nelson, and Congo basins (Fig. 5a). Rainfall is an important variable for

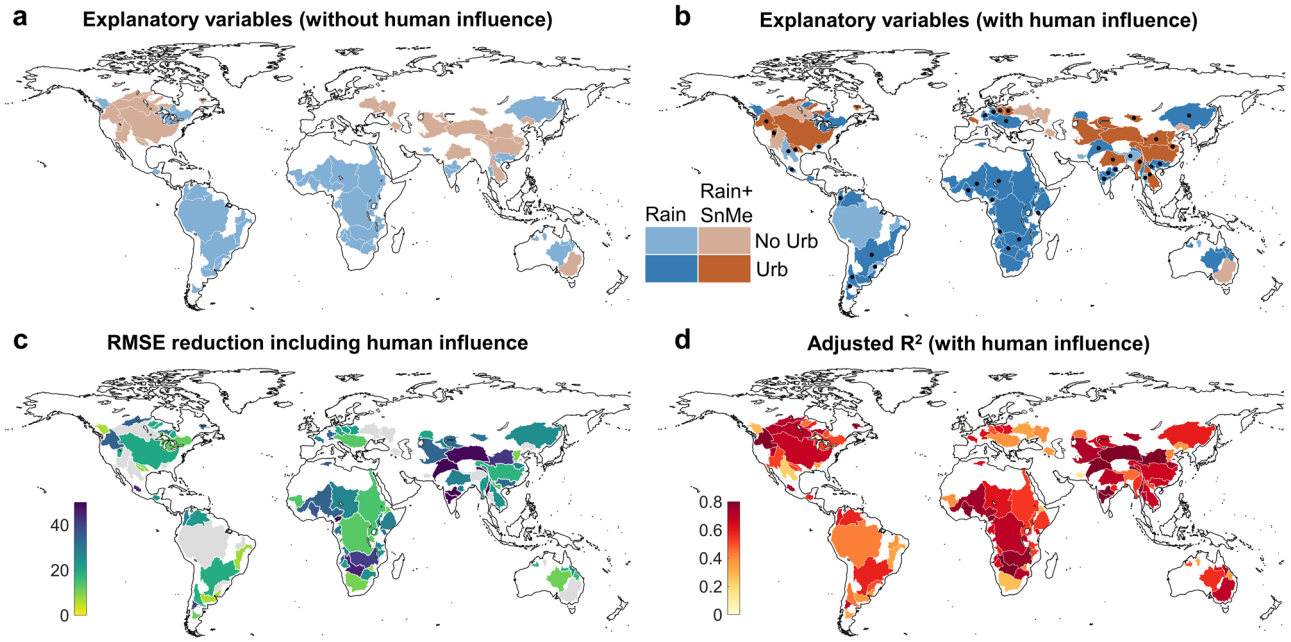

Fig. 5 Outcome of the multiple regression analysis between AMFE (dependent variable) and hydroclimatic variable, urban area, and the maximum capacity of reservoirs (independent variables). Explanatory variables resulting from the multiple linear regression analyses without (**a**), and with (**b**), urban area (Urb), as response variable. The black dots (**b**) indicate the reservoir's maximum capacity as one of the main explanatory variables in addition to rainfall (Rain), and snowmelt (SnMe). **c** Reduction in the root mean square error when including urban area and reservoir capacity in the multiple linear regression analyses. **d** Adjusted R^2 of the multiple linear regression analyses when including urban area and reservoir capacity.

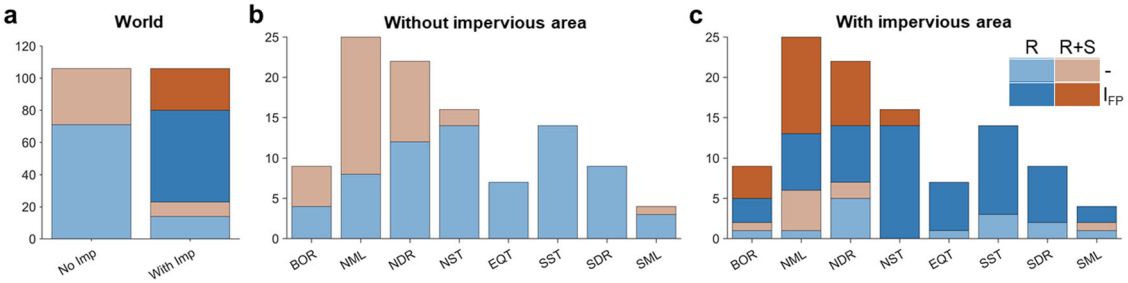

Fig. 6 Distribution of the different explanatory variables for each hydroclimatic regions. a, Global scale. **b**, without, and **c**, with urban area as response variable in the multiple linear regression analyses.

the AMFE in southern and northern sub-tropical basins (Fig. 6b) such as Senegal, Parana, Zambezi, Niger, and Congo as also reported in ref. [46]. In the Ganges, Yellow River, Don, Yangtze, Tarim, Mississippi, and other northern mid-latitude, northern dry and boreal river basins the maximum flood extent can be statistically explained by a combination of rainfall and snowmelt[47].

Our findings indicate that urban area is also a significant variable in the stepwise regression models for 70% of the analyzed river basins (Fig. 5b). Those basins are mainly located in northern mid-latitude areas (Fig. 6), which are characterized by heterogeneous hydroclimatic conditions and by a high percentage (81.4%) of the world's population living within them[41]. Including the urban area in the statistical analysis led to an increase of the explanatory performances of the multiple regression analysis. The results highlight an average reduction of the predictive error (root mean square error, Fig. 5c) up to 27%, with the highest reductions in the Tarim (49%) and Okavango (43%) basins (Fig. 5c). Similarly, the adjusted R^2 (Fig. 5d) tends to increase on average of 71% with respect to the regression analysis without urban area, with maximum values observed in the Tarim (0.85), Indus (0.81), Okavango (0.79), Volta (0.73), and Godavari (0.73) river basins. A sensitivity analysis is then performed to assess the average change of the root mean square error and adjuster R^2 in case of different thresholds of the minimum basin area size (Supplementary Fig. 15).

Rainfall and urban area (dark blue color in Fig. 5a, b) are the main explanatory variables of AMFE in the majority of the river basins (57%), mainly located in northern and southern sub-tropical areas (Fig. 6). This is evident in African river basins, as also showed by previous research focused at a more local level on the Chad[48], Nile[24], Niger[49], Zambezi[24], and Okavango[50] river basins. The combined effect of rainfall and urban area on AMFE is observed also on other major river basins like the Amur, Indus, Godavari, Parana, and Volta river basins[51,52]. In addition to rainfall and snowmelt, urban area (dark brown color in Fig. 5a and b) is a significant variable for 26% of the analyzed river basins. These basins include the Columbia, Mekong, Ganges, Yangtze, Yellow River, Tarim, and Mississippi, as supported by[22,28,53]. In 16% of river basins, climate variability alone can explain changes in AMFE (e.g., in the Amazon, Nelson, Murray, Colorado, and Don river basins). A sensitivity analysis was

performed (Supplementary Fig. 15) to assess the robustness of our findings with respect to the basin area.

In addition to urbanization, other human activities as reservoir construction can alter surface water[39]. As many of the analyzed river basins have large reservoirs, we considered the reservoir maximum capacity as an additional dependent variable in the regression analyses. We found that reservoir maximum capacity is one of the main response variables in 40 river basins (Fig. 5b), of which 5 are influenced by hydroclimatic variables (i.e., in the Brahmaputra and Rio Grande river basins), and 35 influenced by a combination of urban area and hydroclimatic variables (i.e., in the Danube, Yellow River, Ganges, Niger, and Mekong). The majority of the river basins in which reservoir maximum capacity influences changes in AMFE are located in Asia and central western Europe[10]. Such influence can be due to an increase of the flood levels, for the same discharge, downstream the reservoir[54], and to the filling of small reservoirs that affected high-flow and the consequent seasonal surface water within the main river channel[55].

Discussion

We use global high-resolution observational datasets of AMFE and annual impervious surface (used as proxy of urban area) to reveal increasing trends of both variables within river floodplains in the period 1985–2018. High increment values are found in Asian and African river basins. Our exploratory global analysis suggests that hydroclimatic variability alone cannot explain changes in AMFE. Instead, we find that rainfall and urban area together can explain changes in the AMFE for 57% of the analyzed river basins. Including the urban area as response variable in the statistical analyses led to an average increase in the model performances (i.e., adjusted R^2) up to 71%, with a reduction of the predictive error (i.e., root mean square error) up to 30%. In particular, a number of river basins with negative rainfall correlation and increasing trend of AMFE have instead a positive correlation with urban area. Thus, our findings suggest that changes in urbanization, and thus human stress on river basins, together with climatic variability might play an important role increasing global trends of AMFE.

It has been shown that urbanization can increase annual maximum flood and affect statistical properties (e.g., stationarity) of river streamflow[54,56]. However, effects of human presence can be different at different spatial scales. In fact, while urbanization led to an increase in flooding events for small basins[57], urban expansion can affect seasonal surface water extent (i.e., the AMFE) at larger scales due to the complex dynamics between sub-basins[58]. Moreover, we observed that seasonal surface water is more influenced by the reservoirs' maximum capacity than by the hydroclimatic oscillation. Similar relations were also observed by[10] using high-resolution altimetry data for the period 2018–2020.

Urban growth may not only directly affect AMFE as the result of higher surface runoff, but also indirectly due to the maladaptation strategies introduced to reduce drought impacts. For example, increasing urbanization may lead to increasing water demand for urban and agricultural sectors with possible water shortages during drought conditions. As a consequence, changes in agricultural crops and construction of reservoirs could help in reducing water shortages, while they could in turn increase flood vulnerability due to higher surface runoff[59] and inefficient operational release rules[60]. Thus, increasing urbanization could result in the implementation of more flood regulation policies and construction of flood defences, which could increase the presence of seasonal water surface at the expenses of permanent ones.

Increasing trends in urbanization and human presence within floodplains have significantly exacerbated flood risk[61] and the occurrence of drought periods[62], compromising the achievement of the Sustainable Development Goals (SDGs). Capturing the dynamics emerging from the complex interactions between human and water systems is crucial to meet numerous SDGs[63]. For example, the global hotpots characterized by an emerging reciprocal effect between urbanization processes and AMFE changes identified in our study will help addressing SDG11 and promoting resilient and sustainable cities to reduce unplanned urban development on flood impacts. Moreover, the global results found in our study will assist in achieving the SDG6 on protect and restore water-related ecosystems. A better understanding of the effects of anthropogenic drivers on AMFE is therefore needed for developing global policies and guidelines for improving urban planning, mitigation policies, flood risk management, and land-use interventions[64]. In view of the worldwide rapid development of urban areas, this work can inform the process of flood risk management and help improve targeted policy and land-use interventions.

This study has certain limitations. We did not account for the effect of climatic patterns and other types of human actions (e.g., deforestation and agriculture) on the spatio-temporal occurrence of AMFE. Moreover, as the analyses were performed at basin scale, the local influence of urbanization on AMFE is not considered. Despite their potential, the new global datasets used in this study come also with certain limitations. The frequency of flood events included in the Global Surface Water dataset is conditioned by the revisit time of Landsat imagery (8 or 16 days)[41]. This could lead to a possible underestimation of the annual flood maximum extent in areas affected by floods with shorter duration than revisit time, or where flood peak is not captured by Landsat imagery. The Global Artificial Impervious Areas dataset presents large uncertainty in the between 1985 and 2000 due to low availability of Landsat data. In addition, the mapping performances of this dataset could be affected by mixed pixel errors. The authors addressed this issue by assuming stable impervious areas in urban core over the past decades. However, this may not occur in urban renewal processes linked to afforestation and reconstruction in rapidly developing regions. The global GranD database does not include reservoirs with maximum capacity smaller than 0.1 km^3. However, small barriers and reservoir accounts for an important number of the total human-made structures for river regulation and this could highly affect seasonal water extent. Because the GFPLAIN250m dataset provides floodplain extent up to 60°N, river basins of higher altitudes are not included in the analyses.

Future research should focus on unraveling the complexity in the physical and human adaptation responses. Causal inference methods could be used for explaining the emergence of complex dynamics between AMFE and other geomorphological (e.g., changes in river channel), hydrological (e.g., soil moisture, discharge) and socio-economic drivers (e.g., irrigation practices, water uses, structural flood protections, economic value of properties, social welfare measures, flood insurances, etc.)[65,66]. Moreover, integrated earth system frameworks should be developed to represent the dynamics between climate mechanisms, land surface processes, and human dynamics to quantify trade-offs and unintended consequences linked to future flood adaptation actions[67]. Future studies should be also developed to further quantify the effects of land-use change (e.g., deforestation and changes in cropland), changes in the number of reservoirs, spatial distribution of impervious cover[68], uneven urban development across different societal groups, and the influence of flood mapping in (re)distributing floodplains urbanization on flood extent at different spatio-temporal scales. This entails the

synergetic use of empirical local analyses and modeling applications to unravel the complex human-water interplays.

Methods

Data. Five global datasets were exploited to investigate the relationships between global AMFE, impervious area, reservoir presence, and hydroclimatic drivers.

AMFE was derived from the recent Global Surface Water dataset, generated from high-resolution (30 m) Landsat 5, 7, and 8 images[5]. Among the different products of this dataset, we selected the annual maximum water extent available from 1984 to 2018 at the annual time step. The dataset was validated by Pekel et al.[5] using a total of 40,124 control points distributed both geographically (globally), temporally (across the 32 years), and across multiple sensors, reporting less than 5% of omission errors and less than 1% for commission errors. Moreover, the validation showed that less than 1% of the points where water was actually present remained entirely unmapped over time[5]. Non-water, permanent water, and seasonal water (including, for instance, annual floods caused by monsoons and reservoir areas with seasonal oscillations in water extent) are the different surface water classes of the Global Surface Water dataset. We selected only pixels with seasonal surface water to evaluate the annual maximum water extent. Then, we filtered the annual seasonal water with the permanent water extent in the main lakes and wetlands from the Global Lakes and Wetlands Database[69] and the water extent in main river channel estimated as permanent water of the Global Surface Water dataset from 1984 to 2018. The results of this data processing, performed using the Google Earth Engine platform, was assumed to be representative of the AMFE at basin scales.

The AMFE was then assessed only within the floodplains of each major river basins. Floodplains were delineated using the recent GFPLAIN250m dataset proposed in ref. [70] having a spatial resolution of 250 m and spatial extent up to 60°N. This dataset is based on a hydrogeomorphic approach in which the topography is used to directly identify the floodplains as unique morphological entities due to geomorphic and hydrologic processes. One of the advantages of this dataset is that floodplains are identified regardless of the presence or lack of structural flood protection measures (e.g., levee systems). The proper floodplains delineation was fundamental to assess the correlation of maximum flood extent with urban area.

The ERA5 reanalysis dataset was employed to assess the influence of hydroclimatic drivers in shaping AMFE. We considered precipitation and snowmelt as main factors affecting flood extent[47]. Precipitation and snowmelt are estimated as annual maximum, monthly maximum, and total annual values averaged over each river basins. ERA5 freely provides both hourly and monthly estimates of different atmospheric, land and oceanic climate variables from 1979 up to 5 days real-time with about 30 km spatial resolution. Advanced variational data assimilation techniques are used to integrate historical observations within global modeling estimates[71]. It was shown by[72] that precipitation change of ERA5 matches well the observations for all continents, with correlations higher than 90% for Europe and higher than 70% for North America, Asia and Australia. ERA5 data were downloaded from the Copernicus Climate Data Store (https://cds.climate.copernicus.eu/#!/home) from 1985 to 2018 at daily resolution.

The Global Artificial Impervious Areas[43], GAIA, based on Landsat imaginary available on Google Earth Engine, was used to represent the impervious surfaces associated with urbanization and human settlements between 1985 and 2018 with a 30-m spatial resolution. It is worth noting that artificial impervious area has large overlaps with urban area, however, they are not always the same. Urban areas do not include other types of artificial surfaces such as mining fields. However, the GAIA dataset[43] only considered impervious area at urban level, so other types of impervious surface are not included. For each year, the GAIA dataset classifies a pixel as belonging to either an artificial impervious surface (pixel value equal to 1) or to any other land cover type (pixel value equal to 0). We extracted the pixels belonging to artificial impervious surface class using the Google Earth Engine platform and then calculated the artificial impervious area, expressed in km^2, within and outside the floodplains of each river basin. The GAIA dataset showed satisfactory spatial-temporal results when compared with other existing global urban products of different spatial resolution[43]. Overall[43], reported accuracies consistently higher than 89% at the global scale for the GAIA dataset. Moreover, this database can detect impervious areas in small villages which are not detected from coarse-resolution satellite observations[43].

Finally, we used the Global Reservoirs and Dams database (GRanD)[73] to derive the location and reservoir maximum capacity of existing dam and reservoirs with a storage capacity of more than 0.1 km^3.

It is worth noting that because of the high quality of observational datasets and the low and uncorrelated validation errors between global datasets, we can expected a low cumulative error resulting from our findings.

Given the focus on global river flood extent and the resolution of hydroclimatic, we considered a total of 106 perennial rivers (continuous flow all year round) with drainage area bigger than 10^5 km^2 (see Supplementary Data 1). This threshold was selected also to limit the influence of coastal flooding due to tidal effect or storm surge and to discard river basins with comparable areas than the spatial resolution of the ERA5 reanalyzes product to avoid unreliable estimation of precipitation and snowmelt. We did not consider other drivers of AMFE such as river streamflow and soil moisture due to their high relation with the impervious area and to the consequent misleading statistical outcomes.

Trend analysis. We investigate the annual variation of the AMFE, urban area, rainfall, and snowmelt by calculating the trend model of their corresponding annual normalized values. The normalization was performed over the long-term average of the 1985–2018 period to compare the results from basins with different hydroclimatic characteristics. The trends were assessed by means of the adjusted Theil–Sen slope estimator. Annual trends of urban density were assessed by considering the ratio between the annual impervious area and the floodplain area. The resulting annual trends for the 106 analyzed basins are then analyzed at continental scale and over eight climatic representative hydroclimatic regions (or hydrobelts), i.e., boreal, northern mid-latitude, northern dry, northern sub-tropical, equatorial, southern sub-tropical, southern dry, southern mid-latitude[41]. We selected hydrobelts as homogenous regions with similar climatic and hydrological characteristics. Hydrobelts are delineated by natural hydrological basins (similar to our study) and are designed for the analysis of global-scale water-related linked to human alteration[41]. Moreover, the eight hydrobelts are designed in order to maximize the inter-belt differences and minimize the intra-belt hydroclimatic heterogeneity.

Supplementary Fig. 2 shows the location of the analyzed river basins with respect to the global hydrobelts.

The bivariate mapping reported in Fig. 3 was calculated by separately classifying the AMFE, the urban area, and the urban density in three groups according to the 25th, 50th, and 75th percentiles of the corresponding sample of 106 river basins.

Statistical analysis. We first calculated the pair-wise Spearman correlation coefficients and p-values between the AMFE and the explanatory variables (impervious area, rainfall, and snowmelt) for the 106 river basins. Multiple linear regression was then performed to assess which variable could explain the AMFE. Multiple linear regression has been widely used in hydrological and ecological studies for assessing the effect of urbanization on river flow and water quality[74]. Two different multiple linear regressions were performed.

First, only rainfall and snowmelt calculated as annual maximum, monthly maximum, and total annual were considered as explanatory variables. Based on these six different hydroclimatic drivers, a total of 15 possible model outcomes can result from the multiple regression analysis. In order to simplify the visualization of the results, we have grouped the model outcomes having different temporal scales but belonging to the same hydroclimatic variable in a single outcome. For example, if annual maximum rainfall and total annual rainfall are the main explanatory variables of maximum flood extent change in a given river basin, we grouped them as rainfall explanatory variable. Different regression models were generated based on the different combinations of the rainfall and snowmelt variables. Snowmelt was considered as possible explanatory variables in basins with total annual value higher than 10 cm. Moreover, we assumed that maximum flood extent can be explained by either rainfall or by the combination of rainfall and snowmelt as high-latitude basins, mainly driven by snowmelt[75], are not considered in this study. An Augmented Dickey-Fuller test was performed on the residuals of the different multiple linear regression models to discard the ones with non-stationary residuals to avoid spurious correlation leading to misleading statistical results. The Akaike information criterion was used as the objective function to assess the best multiple linear regression model as other indicators like the p-value or the adjusted R^2 may lead to multicollinearity problems and thus misleading results.

Second, once the main explanatory variables were identified, the impervious area and the reservoir's maximum capacity were included to assess the human influence on the maximum flood extent. The results of the multiple linear regression of each river basin are assessed in terms of root mean square error and adjusted R^2.

Data availability

The Global Surface Water Explorer data are publicly available at https://global-surface-water.appspot.com/download or on the Google Earth Engine (https://developers.google.com/earth-engine/datasets/catalog/JRC_GSW1_3_GlobalSurfaceWaterat). The precipitation and snowmelt data can be obtained from the Copernicus Climate Data Store (https://cds.climate.copernicus.eu/#!/home). The Global Artificial Impervious Areas data are publicly available at http://data.ess.tsinghua.edu.cn/. The Global Reservoirs and Dams database (GRanD) is publicly available at https://globaldamwatch.org/grand/. The GFPLAIN250m dataset can be found at https://www.nature.com/articles/sdata2018309#Sec6. The dataset containing all the relevant information about the characteristics of the analyzed river basins, the average values of annual maximum flood extent and urban areas, and the average values of the hydroclimatic variables for the period 1985–2018 are reported in Supplementary Data 1.

Code availability

The scripts used to estimate the annual maximum flood extent, annual urban area, and annual flooded urban area are reported in the supplementary material of the paper.

Received: 20 April 2022; Accepted: 17 October 2022;
Published online: 01 November 2022

References

1. Zhang, W. et al. Increasing precipitation variability on daily-to-multiyear time scales in a warmer world. *Sci. Adv.* **7**, eabf8021 (2021).
2. Swain, D. L., Langenbrunner, B., Neelin, J. D. & Hall, A. Increasing precipitation volatility in twenty-first-century California. *Nat. Clim. Change* **8**, 427–433 (2018).
3. Konapala, G., Mishra, A. K., Wada, Y. & Mann, M. E. Climate change will affect global water availability through compounding changes in seasonal precipitation and evaporation. *Nat. Commun.* **11**, 3044 (2020).
4. Tabari, H. Climate change impact on flood and extreme precipitation increases with water availability. *Sci. Rep.* **10**, 13768 (2020).
5. Pekel, J.-F., Cottam, A., Gorelick, N. & Belward, A. S. High-resolution mapping of global surface water and its long-term changes. *Nature* **540**, 418–422 (2016).
6. Borja, S., Kalantari, Z. & Destouni, G. Global wetting by seasonal surface water over the last decades. *Earth's Future* **8**, e2019EF001449 (2020).
7. Rogger, M. et al. Land use change impacts on floods at the catchment scale: Challenges and opportunities for future research. *Water Resour. Res.* **53**, 5209–5219 (2017).
8. Tao, S. et al. Rapid loss of lakes on the Mongolian Plateau. *Proc. Natl Acad. Sci. USA* **112**, 2281–2286 (2015).
9. Timpe, K. & Kaplan, D. The changing hydrology of a dammed Amazon. *Sci. Adv.* **3**, e1700611 (2017).
10. Cooley, S. W., Ryan, J. C. & Smith, L. C. Human alteration of global surface water storage variability. *Nature* **591**, 78–81 (2021).
11. Suriya, S. & Mudgal, B. V. Impact of urbanization on flooding: the Thirusoolam sub watershed–a case study. *J. Hydrol.* **412**, 210–219 (2012).
12. Bruwier, M. et al. Influence of urban pattern on inundation flow in floodplains of lowland rivers. *Sci. Total Environ.* **622–623**, 446–458 (2018).
13. Nichols, K. K. et al. Quantifying urban land use and runoff changes through service-learning hydrology projects. *J. Geosci. Educ.* **51**, 365–372 (2003).
14. Boulange, J., Hanasaki, N., Yamazaki, D. & Pokhrel, Y. Role of dams in reducing global flood exposure under climate change. *Nat. Commun.* **12**, 417 (2021).
15. Deemer, B. R. et al. Greenhouse gas emissions from reservoir water surfaces: a new global synthesis. *BioScience* **66**, 949–964 (2016).
16. Liu, X. et al. High-spatiotemporal-resolution mapping of global urban change from 1985 to 2015. *Nat. Sustain.* **3**, 564–570 (2020).
17. Andreadis, K. M. et al. Urbanizing the floodplain: global changes of imperviousness in flood-prone areas. *Environ. Res. Lett.* **17**, 104024 (2022)
18. Ceola, S., Laio, F. & Montanari, A. Satellite nighttime lights reveal increasing human exposure to floods worldwide. *Geophys. Res. Lett.* **41**, 7184–7190 (2014).
19. Sofia, G., Roder, G., Dalla Fontana, G. & Tarolli, P. Flood dynamics in urbanised landscapes: 100 years of climate and humans' interaction. *Sci. Rep.* **7**, 1–12 (2017).
20. van Vliet, J., Eitelberg, D. A. & Verburg, P. H. A global analysis of land take in cropland areas and production displacement from urbanization. *Global Environ. Change* **43**, 107–115 (2017).
21. Güneralp, B., Güneralp, İ. & Liu, Y. Changing global patterns of urban exposure to flood and drought hazards. *Global Environ. Change* **31**, 217–225 (2015).
22. Huong, H. T. L. & Pathirana, A. Urbanization and climate change impacts on future urban flooding in Can Tho city, Vietnam. *Hydrol. Earth Syst. Sci.* **17**, 379–394 (2013).
23. Zhang, W., Villarini, G., Vecchi, G. A. & Smith, J. A. Urbanization exacerbated the rainfall and flooding caused by hurricane Harvey in Houston. *Nature* **563**, 384–388 (2018).
24. Douglas, I. Flooding in African cities, scales of causes, teleconnections, risks, vulnerability and impacts. *Int. J. Disaster Risk Reduc.* **26**, 34–42 (2017).
25. Nirupama, N. & Simonovic, S. P. Increase of flood risk due to urbanisation: a Canadian example. *Nat. Hazards* **40**, 25 (2006).
26. Remondi, F., Burlando, P. & Vollmer, D. Exploring the hydrological impact of increasing urbanisation on a tropical river catchment of the metropolitan Jakarta, Indonesia. *Sustain. Cities Soc.* **20**, 210–221 (2016).
27. Miller, J. D. & Hutchins, M. The impacts of urbanisation and climate change on urban flooding and urban water quality: A review of the evidence concerning the United Kingdom. *J. Hydrol. Regional Studies* **12**, 345–362 (2017).
28. Blum, A. G., Ferraro, P. J., Archfield, S. A. & Ryberg, K. R. Causal effect of impervious cover on annual flood magnitude for the United States. *Geophys. Res. Lett.* **47**, e2019GL086480 (2020).
29. Jha, A. K., Bloch, R. & Lamond, J. *Cities and Flooding: A Guide to Integrated Urban Flood Risk Management for the 21st Century* (The World Bank, 2012).
30. Junk, W. J. et al. Current state of knowledge regarding the world's wetlands and their future under global climate change: a synthesis. *Aquat. Sci.* **75**, 151–167 (2013).
31. Wada, Y., Wisser, D. & Bierkens, M. F. P. Global modeling of withdrawal, allocation and consumptive use of surface water and groundwater resources. *Earth Syst. Dyn.* **5**, 15–40 (2014).
32. Zarfl, C., Lumsdon, A. E., Berlekamp, J., Tydecks, L. & Tockner, K. A global boom in hydropower dam construction. *Aquat. Sci.* **77**, 161–170 (2015).
33. Nohrstedt, D., Mazzoleni, M., Parker, C. F. & Di Baldassarre, G. Exposure to natural hazard events unassociated with policy change for improved disaster risk reduction. *Nat. Commun.* **12**, 193 (2021).
34. Shuster, W. D., Bonta, J., Thurston, H., Warnemuende, E. & Smith, D. R. Impacts of impervious surface on watershed hydrology: a review. *Urban Water J.* **2**, 263–275 (2005).
35. Prosdocimi, I., Kjeldsen, T. R. & Miller, J. D. Detection and attribution of urbanization effect on flood extremes using nonstationary flood-frequency models. *Water Resour. Res.* **51**, 4244–4262 (2015).
36. Du, S., Shi, P., Van Rompaey, A. & Wen, J. Quantifying the impact of impervious surface location on flood peak discharge in urban areas. *Nat. Hazards* **76**, 1457–1471 (2015).
37. Sohn, W., Kim, J.-H., Li, M.-H., Brown, R. D. & Jaber, F. H. How does increasing impervious surfaces affect urban flooding in response to climate variability? *Ecol. Indicators* **118**, 106774 (2020).
38. Miller, J. D. et al. Assessing the impact of urbanization on storm runoff in a peri-urban catchment using historical change in impervious cover. *J. Hydrol.* **515**, 59–70 (2014).
39. Zou, Z. et al. Divergent trends of open-surface water body area in the contiguous United States from 1984 to 2016. *Proc. Natl Acad. Sci. USA* **115**, 3810–3815 (2018).
40. Wang, X. et al. Gainers and losers of surface and terrestrial water resources in China during 1989–2016. *Nat. Commun.* **11**, 3471 (2020).
41. Meybeck, M., Kummu, M. & Dürr, H. H. Global hydrobelts and hydroregions: improved reporting scale for water-related issues? *Hydrol. Earth Syst. Sci.* **17**, 1093–1111 (2013).
42. Dryden, R., Anand, M., Lehner, B. & Fluet-Chouinard, E. Do we prioritize floodplains for development and farming? Mapping global dependence and exposure to inundation. *Global Environ. Change* **71**, 102370 (2021).
43. Gong, P. et al. Annual maps of global artificial impervious area (GAIA) between 1985 and 2018. *Remote Sens. Environ.* **236**, 111510 (2020).
44. Mård, J., Baldassarre, G. D. & Mazzoleni, M. Nighttime light data reveal how flood protection shapes human proximity to rivers. *Sci. Adv.* **4**, eaar5779 (2018).
45. Berghuijs, W. R., Woods, R. A., Hutton, C. J. & Sivapalan, M. Dominant flood generating mechanisms across the United States. *Geophys. Res. Lett.* **43**, 4382–4390 (2016).
46. Tramblay, Y., Villarini, G. & Zhang, W. Observed changes in flood hazard in Africa. *Environ. Res. Lett.* **15**, 1040b5 (2020).
47. Mao, Y. et al. Flood inundation generation mechanisms and their changes in 1953–2004 in global major river basins. *J. Geophys. Res. Atmos.* **124**, 11672–11692 (2019).
48. Adeyeri, O. E., Laux, P., Lawin, A. E. & Arnault, J. Assessing the impact of human activities and rainfall variability on the river discharge of Komadugu-Yobe Basin, Lake Chad Area. *Environ. Earth Sci.* **79**, 143 (2020).
49. Aich, V. et al. Flood projections within the Niger River Basin under future land use and climate change. *Science of The Total Environment* **562**, 666–677 (2016).
50. Andersson, L. et al. Impact of climate change and development scenarios on flow patterns in the Okavango River. *J. Hydrol.* **331**, 43–57 (2006).
51. Koronkevich, N. I. et al. Assessing the anthropogenic impact on the water resources of Russia. *Her. Russ. Acad. Sci.* **89**, 287–297 (2019).
52. Bisht, D. S., Chatterjee, C., Raghuwanshi, N. S. & Sridhar, V. Spatio-temporal trends of rainfall across Indian river basins. *Theor. Appl. Climatol.* **132**, 419–436 (2018).
53. Misra, A. K. Impact of urbanization on the hydrology of Ganga Basin (India). *Water Resour. Manag.t* **25**, 705–719 (2011).
54. Yang, Y. et al. Influence of large reservoir operation on water-levels and flows in reaches below dam: case study of the three gorges reservoir. *Sci. Rep.* **7**, 15640 (2017).
55. Shin, S. et al. High resolution modeling of river-floodplain-reservoir inundation dynamics in the Mekong River Basin. *Water Resour. Res.* **56**, e2019WR026449 (2020).
56. Vogel, R. M., Yaindl, C. & Walter, M. Nonstationarity: flood magnification and recurrence reduction factors in the United States 1. *J. Am. Water Resour. Assoc.* **47**, 464–474 (2011).
57. Merz, B. et al. Causes, impacts and patterns of disastrous river floods. *Nat. Rev. Earth Environ.* **2**, 592–609 (2021).

58. Villarini, G. & Wasko, C. Humans, climate and streamflow. *Nat. Clim. Change* **11**, 725–726 (2021).
59. O'Connell, P. E., Ewen, J., O'Donnell, G. & Quinn, P. Is there a link between agricultural land-use management and flooding?, *Hydrol. Earth Syst. Sci.* **11**, 96–107 (2007).
60. Van den Honert, R. C. & McAneney, J. The 2011 Brisbane floods: causes, impacts and implications. *Water* **3**, 1149–1173 (2011).
61. Dottori, F. et al. Increased human and economic losses from river flooding with anthropogenic warming. *Nat. Clim. Change* **8**, 781–786 (2018).
62. Chiang, F., Mazdiyasni, O. & AghaKouchak, A. Evidence of anthropogenic impacts on global drought frequency, duration, and intensity. *Nat. Commun.* **12**, 1–10 (2021).
63. Di Baldassarre, G. et al. Sociohydrology: scientific challenges in addressing the sustainable development goals. *Water Resour. Res.* **55**, 6327–6355 (2019).
64. Hemmati, M., Ellingwood, B. R. & Mahmoud, H. N. The role of urban growth in resilience of communities under flood risk. *Earth's Future* **8**, e2019EF001382 (2020).
65. d'Amour, C. B. et al. Future urban land expansion and implications for global croplands. *Proc. Natl Acad. Sci. USA* **114**, 8939–8944 (2017).
66. Cattaneo, A., Nelson, A. & McMenomy, T. Global mapping of urban–rural catchment areas reveals unequal access to services. *Proc. Natl Acad. Sci. USA* **118**, e2011990118 (2021).
67. Harrigan, S., Cloke, H. & Pappenberger, F. Innovating global hydrological prediction through an Earth system approach. *WMO Bull.* **69**, 1 (2020).
68. Debbage, N. & Shepherd, J. M. The influence of urban development patterns on streamflow characteristics in the charlanta megaregion. *Water Resour. Res.* **54**, 3728–3747 (2018).
69. Lehner, B. & Döll, P. Development and validation of a global database of lakes, reservoirs and wetlands. *J. Hydrol.* **296**, 1–22 (2004).
70. Nardi, F., Annis, A., Di Baldassarre, G., Vivoni, E. R. & Grimaldi, S. GFPLAIN250m, a global high-resolution dataset of Earth's floodplains. *Sci. Data* **6**, 180309 (2019).
71. Hersbach, H. et al. The ERA5 global reanalysis. *Quart. J. Royal Meteorol. Soc.* **146**, 1999–2049 (2020).
72. Bell, B. et al. The ERA5 global reanalysis: preliminary extension to 1950. *Quart. J. Royal Meteorol. Soc.* **147**, 4186–4227 (2021).
73. Lehner, B. et al. High-resolution mapping of the world's reservoirs and dams for sustainable river-flow management. *Front. Ecol. Environ.* **9**, 494–502 (2011).
74. Lin, Y.-P., Lin, Y.-B., Wang, Y.-T. & Hong, N.-M. Monitoring and predicting land-use changes and the hydrology of the urbanized paochiao watershed in Taiwan using remote sensing data, urban growth models and a hydrological model. *Sensors* **8**, 658–680 (2008).
75. Adam, J. C., Hamlet, A. F. & Lettenmaier, D. P. Implications of global climate change for snowmelt hydrology in the twenty-first century. *Hydrol. Processes* **23**, 962–972 (2009).

Acknowledgements

This work was developed within the activities of the working group on Changes in Flood Risk of the Panta Rhei research initiative of the International Association of Hydrological Sciences. M.M. and G.D.B. were funded by the European Research Council within the project HydroSocialExtremes (grant agreement no. 771678), Formas (the Swedish Research Council for Environment, Agricultural Sciences, and Spatial Planning) and by the Centre of Natural Hazards and Disaster Science. H.L.C. was supported by the UK's Natural Environment Research Council (NERC) EVOFLOOD project (The Evolution of Global Flood Risk, grant number NE/S015590/1).

Author contributions

M.M. and G.D.B. designed research; M.M. performed research, collected data, and analyzed the data; M.M., F.D., H.L.C., and G.D.B. analyzed the results; M.M. wrote the manuscript; F.D., H.L.C., and G.D.B. substantially contributed to the manuscript.

Competing interests

The authors declare no competing interests.

Additional information

Supplementary information The online version contains supplementary material available at https://doi.org/10.1038/s43247-022-00598-0.

Correspondence and requests for materials should be addressed to Maurizio Mazzoleni.

Peer review information *Communications Earth & Environment* thanks Gustavo Coelho, Benjamin P. Warner and the other, anonymous, reviewer(s) for their contribution to the peer review of this work. Primary Handling Editors: Michael Bank, Joe Aslin and Clare Davis. Peer reviewer reports are available.

Reprints and permission information is available at http://www.nature.com/reprints

Publisher's note Springer Nature remains neutral with regard to jurisdictional claims in published maps and institutional affiliations.

Open Access This article is licensed under a Creative Commons Attribution 4.0 International License, which permits use, sharing, adaptation, distribution and reproduction in any medium or format, as long as you give appropriate credit to the original author(s) and the source, provide a link to the Creative Commons license, and indicate if changes were made. The images or other third party material in this article are included in the article's Creative Commons license, unless indicated otherwise in a credit line to the material. If material is not included in the article's Creative Commons license and your intended use is not permitted by statutory regulation or exceeds the permitted use, you will need to obtain permission directly from the copyright holder. To view a copy of this license, visit http://creativecommons.org/licenses/by/4.0/.

© The Author(s) 2022